JOURNAL OF Applied Polymer SCIENCE

Mechanical, Morphological, and Thermal Properties of Nanotalc Reinforced PA6/SEBS-*g*-MA Composites

Hemlata, S. N. Maiti
Centre for Polymer Science and Engineering, Indian Institute of Technology Delhi, Hauz Khas, New Delhi 110016, India
Correspondence to: S. N. Maiti (E-mail: maiti@polymers.iitd.ac.in)

ABSTRACT: Ternary butylene-styrene-*g*-maleic anhydride (SEBS-*g*-MA) (100/20 w/w) blend with varying content of nanotalc (1, 3, and 5 wt %) were prepared by melt compounding followed by injection molding. Thermal properties were investigated by thermogravimetric analysis (TGA) and the results show that the thermal properties of nanocomposites are slightly improved by the addition of nanotalc content. The morphology of nanocomposites using wide angle X-ray diffraction (WAXD) and transmission electron microscopy (TEM) revealed the delamination of talc layers in the ternary nanocomposites. The dynamic mechanical properties of the samples were analyzed by using dynamic mechanical thermal analyzer (DMTA). The results show that the storage modulus of the blend monotonically increased while tan δ curve show the diffuse pattern with the nanotalc content. The mechanical properties of PA6/SEBS-*g*-MA nanocomposites were studied by tensile, flexural, and impact tests. The tensile and flexural properties continuously increased while izod impact and elongation-at-break decreased with nanotalc content. Various theoretical predictive models were used to correlate tensile modulus with the experimental data. The experimental data shows the positive deviation with the applied models. Bela Pukanszky model has been used to calculate the value of parameter B by employing tensile strength data. © 2014 Wiley Periodicals, Inc. J. Appl. Polym. Sci. **2015**, *132*, 41381.

KEYWORDS: mechanical properties; morphology; nanostructured polymers; polyamides; theory and modeling

Received 1 May 2014; accepted 6 August 2014
DOI: 10.1002/app.41381

INTRODUCTION

In recent years, research in the field of polymer nanocomposites have received special attention by both academic and industrial society because of their improved properties at very low filler concentrations as compared to conventional micro and macrocomposite materials. The typical improved properties include mechanical properties, dimensional, and thermal stability, flame retardency and barrier properties.[1,2]

However, the nanocomposites based on PA6 have received much attention and a lot of research has been devoted because of its polar nature eases in obtaining better dispersion of nanofiller. The pioneering work of Toyota researchers was conducted on PA6/montmorillonite obtained by *in situ* intercalative polymerization.[3,4] They also reported a wide range of studies on the preparation of exfoliated polymer-clay hybrid nanocomposites such as polyimides, polyesters, polypropylene, epoxies, and elastomers.[5–17] The literature based on polymer nanocomposites mainly focuses on the use of clay and layered silicate because of easy availability.[18,19] This article investigates the effect of nanotalc as reinforcing filler for PA6. Talc is a hydrated magnesium silicate with a typical molecular formula of $Mg_3Si_4O_{10}(OH)_2$.[20] Talc is a 2 : 1 layered phyllosilicate and the crystal structure is composed of octahedral magnesium brucite sheet ($Mg_{12}O_{12}H_4$) sandwitched between two tetrahedral sheets of silica.[21] The talc layers are electrically neutral and held together by weak van der Waals forces. Talc is believed to be delaminated at a low shear rate due to its weak van der Waals forces between the layers which allow the sliding of brucite and silica layers over each other.

PA6 is an important semicrystalline thermoplastic and finds wide range of applications due to its attractive combination of good processability, high tensile properties, and chemical resistance. However, PA6 is a pseudoductile polymer due to its high crack initiation energy and low crack propagation resistance in the presence of notch, which limits its end use applications.[22] To overcome its poor notched impact strength, blending with various elastomers such as SEBS/SEBS-*g*-MA,[23–25] acrylonitrile butadiene styrene (ABS),[26–29] ethylene propylene rubber (EPR)/EPR-*g*-MA,[30–32] epoxidized ethylene propylene diene rubber[33] and epoxidized natural rubber[34] is a well known method. Blending with SEBS-*g*-MA could enhance the impact strength of PA6, but strength and stiffness characteristics decreased to a

Table I. Raw Materials and Their Characteristics

Material	Grade and supplier	Characteristics
PA6	M28RC, GSFC Ltd	MFI (230°C, 2.16 kg. load): 28 g/10 min, density 1.14 g/cm^3
SEBS-*g*-MA	Kraton FG1901X, Shell chemical company	MFI (230°C, 5 kg load): 14–22 g/10 min and density 0.91 g/cm^3
Nanotalc	POS75, Technano materials Pvt. Ltd India	Average particle size:135 nm, light gray color, density 2.75 g/cm^3

significant extent.[24,35–38] A new approach in the field of polymer nanocomposites based on binary blends has been directed toward improving the balance level of toughness-to-stiffness that can be achieved by the addition of nanofillers.[39–42] Many researchers have investigated the polymer/clay nanocomposites toughened with thermoplastic elastomers.

Gonzalez et al.[43,44] investigated PA6/SEBS-*g*-MA/OMMT ternary nanocomposites where rigidifying effect of the clay and the toughening effect of the SEBS-*g*-MA came together. They reported that super tough PA6/clay nanocomposites could be obtained with 44% increase of modulus as compared to pure PA6 at 30% SEBS-*g*-MA content and rubber particle size generally decreased when maleic anhydride content of SEBS increased the ductile-brittle transition temperature. In addition, Gonzalez et al.[42] studied the effect of processing sequence and critical particle distance in PA6-clay/SEBS-*g*-MA nanocomposites. The analysis of the variation of critical interparticle distance (τ) indicates that it depends on the elastic modulus of the matrix and on the interfacial adhesion leading to smaller τ values. Ahn and Paul et al.[45] studied the ductile-brittle transition temperature (T_{db}) of nylon6/organoclay nanocomposites toughened with maleic anhydride grafted ethylene-propylene rubber and showed that T_{db} increased with organoclay content and decreased with rubber content. The ductile-brittle transition was reduced from 55°C to −10°C and the notched izod impact strength value was substantially enhanced from 49 to 951 J/m by adding only 20 wt % EPR-*g*-MA in nylon6/organoclay nanocomposites (3.2 wt % organoclay). Khatua et al.[46] found that the dispersed domain size of EPR phase in the nylon6 matrix decreased significantly even if a small amount of organoclay incorporated. The exfoliation of clay platelets in the matrix prevents coalescence of the dispersed phase.

Chiu et al.[40] investigated the PA6/organoclay nanocompsotes with a maleated polyethylene-octene elastomer (POE-*g*-MA). They found that the addition of POE-*g*-MA to PA6/organoclay nanocomposites leads to decrease in tensile strength and modulus while elongation at break and impact strength increased significantly. This remarkable enhancement may be attributed to the interaction between maleic anhydride groups of POE-*g*-MA and amine end groups of PA6.

Sharif et al.[47] studied epoxidized natural rubber (ENR-50) toughened polymamide6/halloysite nanotubes (PA6/HNTs) nanocomposites and observed that super tough PA6/HNTs/ENR-50 ternary nanocomposites were achieved at 4 wt % halloysite and 15 wt % ENR-50 rubber content. He et al.[48] investigated PA6/SEBS-*g*-MA/organoclay (DK5) composites with glycidyl methacrylate as a compatibilizer. The influence of maleation, organoclay (DK5), and glycidyl methacrylate on the adhesion, mechanical properties, crystallization, and rheological properties were observed. Satisfactory balanced mechanical properties of nanocomposites could be achieved in presence of glycidyl methacrylate (GMA).

The effect of nanotalc on binary PA6/talc and ternary PA6/ethylene butyl acrylate (EBA)-*g*-MA/EBA/talc nanocomposites was investigated by Balamurugan and Maiti.[49] It is observed that binary and ternary nanocomposites registered high improvement in the stiffness/strength related properties at lower nanotalc content of 1 wt %. The improvement in strength related properties is due to the retention of high aspect ratio of nanotalc and ability of nanotalc particles to orient along the melt flow direction in the nanocomposites. The strain related properties of binary nanocomposites decreases but remain higher than that of ternary nanocomposites. The enhanced flow behavior of both binary and ternary nanocomposites was also observed that may be due to orientation and sliding of the talc particles during high shear flow.

The addition of clay in to PA6/elastomers blends leads to significant reduction of the toughness, which may be attributed to the worsening interfacial adhesion and blocking effect on the stress volume overlap between the elastomer particles in a large extent when the clay content is high.[50] The phase adhesion between the phases strongly influences the final properties of the material. The improved phase adhesion between PA6 and the elastomers leads to loss of toughness.[51]

The objective of this work is to investigate mechanical, morphological, and thermal properties of nanotalc reinforced PA6/SEBS-*g*-MA composites. Thermal properties of PA6/SEBS-*g*-MA nanocomposites containing 1, 3, and 5 nanotalc content were characterized by means of TGA and DMA analysis. Dispersion of nanotalc in the nanocomposites was analyzed by the TEM and WAXD techniques. Tensile, impact and flexural tests were used to evaluate the mechanical properties of nanocomposites. Tensile modulus and strength data were compared with theoretical predictive models.

EXPERIMENTAL

Melt Compounding

The details of materials used in this study are given in Table I. PA6 and SEBS-*g*-MA were dried in vacuum at 80°C for 12 h; nanotalc was dried at 100°C for 4 h. The nanocomposites were melt processed in two stages. In the first stage of compounding, PA6/nanotalc master batch was prepared in a corotating twin

Table II. Compositions of Nanocomposites

Polyamide6 (pbw)	SEBS-*g*-MA(phr)	Nanotalc (wt %)	Sample code
100	0	0	PA6
100	20	0	NC0
100	20	1	NC1
100	20	3	NC3
100	20	5	NC5

screw extruder of Thermo Scientific, Prism Euro Lab (L/D = 40) at a screw speed 300 rpm and temperature range 220–260°C from the feed zone to the die zone. In the second stage of compounding, PA6 and SEBS-*g*-MA were added in constant weight proportions of PA6 and SEBS-*g*-MA (100/20) with calculated quantity of PA6/nanotalc master batch to prepare PA6/SEBS-*g*-MA/nanotalc (1, 3, and 5 wt %) ternary nanocomposites Table II. The extruded pellets were dried for 12 h at 80°C under vacuum and then injection molded on an L&T Demag Machine (Model-PFY40LNC4P), the temperature profile from feed zone to the nozzle was 235–265°C at a screw speed 90, while maintaining the mold temperature at 30 ± 2°C.

The volume fraction of the filler (Φ_f) is determined by theoretical method, which is as follows:

$$\Phi_f = \frac{W_f/\rho_f}{W_m/\rho_m + W_d/\rho_d + W_f/\rho_f} \quad (1)$$

where W_f, W_m, and W_d denote the mass of the filler, the matrix polymer and that of the dispersed phase, while ρ_f, ρ_m, and ρ_d are the densities of the filler, PA6 and SEBS-*g*-MA copolymer, respectively.

Characterization and Measurement Techniques

Thermogravimetric Analysis. Thermal degradation analysis of samples were carried out on a TGA instrument of Perkin Elmer Pyris6 system in a dynamic atmosphere of nitrogen from ambient temperature (30°C) to 750°C at a heating rate of 20°C/min. The primary TGA traces were obtained as the plots of residual mass (%) against the temperature.

Wide Angle X-ray Diffraction. Wide angle X-ray diffraction (WAXD) measurements were carried out on the injection molded rectangular block samples of 12 × 10 × 3 mm^3 to characterize the crystal structure of the samples. The dispersion and delamination of silicate layer of nanotalc in the polymer matrix analyzed. The measurements were done on a Phillips X-ray diffraction Machine, PAN Analytical Diffractometer (40 kV, 30 MA) at a radial scattering range of 2–35° using CuKα radiation.

Transmission Electron Microscopy (TEM). TEM measurements were performed on microtomed sections, from the middle positions of the tensile molded bars in the flow direction. Ultrathin sections were cryogenically cut with a glass knife of 45° cutting edge by using Leica Ultracut UCT microtome. TEM analysis was carried out on high resolution TEM JEOL-2100 (Tokyo, Japan) having LaB6 filament with an accelerating voltage of 200 kV.

Dynamic Mechanical Analysis (DMA). The DMA measurements were performed on tensile specimens with nominal dimensions 27 × 10 × 3 mm^3 using an Q800, TA instrument, USA, to assess the storage modulus, loss modulus, and the mechanical loss factor (tan δ). The temperature range was from −80°C to −125°C at an oscillatory frequency of 1 Hz and heating rate of 5°C/min.

Mechanical Properties. Tensile testing was performed on a Zwick Z010 universal testing machine according to ASTM D638 test procedure with the crosshead separation of 6 cm and crosshead speed of 50 mm/min[52] flexural test were carried out according to ASTM D790[53] test method and the izod impact tests were conducted on a notched samples using Atsfaar IBM15 impact tester following ASTM D256 test procedure.[54] Averages of at least five samples were tested for each composition. The tests were performed at ambient temperature 30 ± 2°C.

RESULTS AND DISCUSSION

Thermogravimetric Analysis

Figure 1 shows the TGA traces of PA6, PA6/SEBS-*g*-MA blend and its nanocomposites. The thermal degradation parameters such as onset degradation temperature (T_{onset}) at 5% weight loss, final decomposition temperature (T_f) and temperature at maximum rate of weight loss (T_{max}) are listed in Table III. It can be observed that all the samples displayed single step degradation process. The onset decomposition temperature and final decomposition temperature for PA6/SEBS-*g*-MA blend appeared at 435.6 and 476.8°C, whereas for nanocomposites the temperatures were observed 435.9–437.9°C and 476.7–480.1°C. This may be attributed to interaction between nanotalc and PA6/SEBS-*g*-MA. It is already reported in literature that thermal stability of materials can be improved by the incorporation of inorganic materials according to their thermal stability and barrier properties,[55] but the incorporation of nanotalc in PA6/SEBS-*g*-MA did not show significant change. Similar results

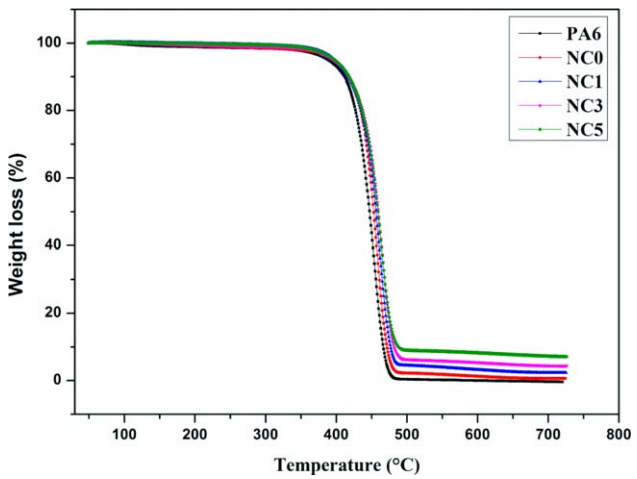

Figure 1. TGA scans for PA6, PA6/SEBS-*g*-MA blend, and PA6/SEBS-*g*-MA/nanotalc composites. [Color figure can be viewed in the online issue, which is available at wileyonlinelibrary.com.]

Table III. Values of TGA Parameters T_{onset}, T_{max}, and T_f in PA6, PA6/SEBS-*g*-MA, and PA6/SEBS-*g*-MA/Nanotalc Composites

Sample code	Thermogravimetric data			
	T_{onset} (°C)	T_{max} (°C)	T_f (°C)	Char yield (%)
PA6	430.0	459.3	476.9	99.89
NC0	435.6	459.1	476.8	98.26
NC1	435.9	459.2	476.7	97.52
NC3	437.76	464.9	479.4	95.32
NC5	437.9	465.1	480.1	92.62

were reported in MMT filled PA6 composites[56] and nanotalc reinforced PA6 composites.[57]

Morphological Characterization

Wide Angle X-ray Diffraction. In WAXD pattern, Figure 2, PA6 and the blend matrix exhibit broad and intense peak at $2\theta = 21.4°$ and 21.8°, which are attributed to the 001 crystal planes of γ_2-phase of PA6.[58–60] Therefore, it is evident that the γ_2 phase is the dominant crystalline phase in PA6 and PA6/SEBS-*g*-MA blend. In addition, two diffraction peaks at 10.2° and 29.18° are observed; however, the intensities was not very strong. The peak at 10.2° is associated with (020) crystal plane of γ_1 phase while the peak at 29.18° is still debated.[61,62] Nanotalc shows a characteristic diffraction peak (d_{001}) at 9.5° corresponding to a basal spacing of 9.54 A°.[63] At $2\theta = 2–10°$, the absence of diffraction peak (d_{001}) of nanotalc in the blend suggests that delamination of talc has occurred. Upon addition of nanotalc a new diffraction peaks appeared at $2\theta = 24.0°$, which is associated with the (002/202) crystal plane of α_2 crystals of PA6.[60] The diffraction intensities of γ_2 (001) and α2 (002/202) reflections decrease with nanotalc content and diffuse pattern of α and γ crystal phase appeared in the nanocomposites, implying significant change in the crystal structure of PA6. Moreover, the addition of nanotalc induces the formation of γ_1 crystalline phase of PA6 and the intensity of (020) diffraction peak becomes relatively stronger as compared to the intensities of the (001) and (002) crystal planes. Hence, it can be observed that the addition of nanotalc further enhances the formation of γ_1 crystalline form. This may be attributed to that in the presence of nanotalc the molecular chains have to twist away from the zigzag plane to from hydrogen bonding in parallel direction giving rise to lesser chain interaction which favors pseudohexagonal crystal form.[64] The existence of γ1 crystalline form also has been reported in PA6/glass bead, PA6/sepiolite and PA6/layered silicate composites.[65–67] The diffraction intensity of the peak at $2\theta = 29.18°$ became more prominent with increasing nanotalc content. The appearance of this crystalline peak (29°) has been reported by Zhao et al. for PA6/montmorillonite nanocomposites and termed it as a high temperature crystalline peak.[68]

Transmission Electron Microscopy Analysis. Figure 3 shows the HRTEM images of nanotalc and nanocomposites with varying nanotalc contents. The dark lines represent the intersection of layered silicate while the gray and white base corresponds to PA6 and SEBS-*g*-MA phase, respectively. The micrographs show partially exfoliated/intercalated nanocomposite structures of talc platelets with random distribution and no indication of aggregate tactoids have been observed even at these higher magnifications. It can be observed that exfoliation/intercalation of nanotalc occurs in both the phases (PA6, SEBS-*g*-MA). This may be attributed to that nanotalc has a silanol group, which has good affinity for polar amide group of PA6 and maleic anhydride group of SEBS-*g*-MA, which may lead to possible interaction by hydrogen bonding between nanotalc and the functional groups of the polymers.

Dynamic Mechanical Analysis. Figure 4(a) shows the plot of storage modulus of PA6, PA6/SEBS-*g*-MA blend and its nanocomposites. The storage modulus for all the samples decayed with increasing temperature, implying increase in segmental motion of polymer chain with increasing temperature.[69] The storage modulus of PA6 decreases with the addition of SEBS-*g*-MA content indicating the decreased ability of material to store mechanical energy. This may be attributed to the softening of PA6 matrix in presence of low modulus SEBS-*g*-MA elastomeric phase, which is also in agreement with the tensile modulus. It can be seen that storage modulus of PA6/SEBS-*g*-MA blend significantly increases with the talc content at the entire measured temperature range. This may be attributed to the reinforcing effect of nanotalc because of intercalated/exfoliated structure that allows better stress transfer at the interface.[70]

The plot of tan δ as a function of temperature is depicted in Figure 4(b). It can be seen that the damping behavior of PA6/SEBS-*g*-MA blend is slightly increased as compared to PA6 because of higher damping behavior of SEBS-*g*-MA. The glass transition temperature (T_g) of PA6, SEBS-*g*-MA, PA6/SEBS-*g*-MA blend and its related nanocomposites derived from tan δ curve [Figure 4(b)]. PA6 shows single dynamic relaxation peak at 48.73°C, which is attributed to the α relaxation peak of PA6.[71] SEBS-*g*-MA shows two dynamic relaxation peaks at −32.53 and 96.9°C, which may be associated to the β and α peak. The β relaxation peak is appeared due to ethylene/butylene segments of SEBS-*g*-MA and α is due to PS blocks in

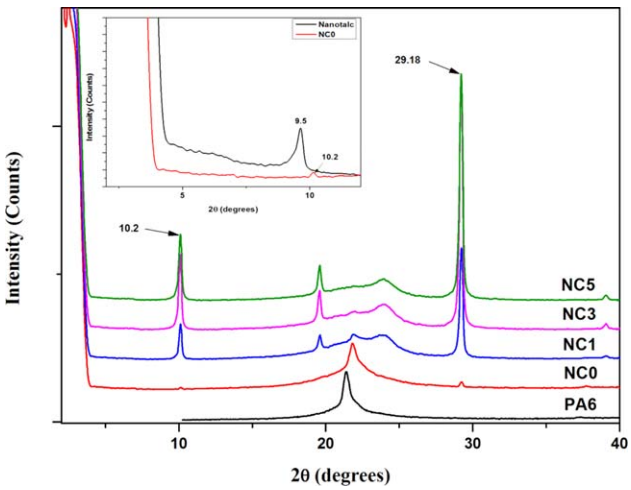

Figure 2. Wide angle diffraction pattern of PA6, nanotalc, PA6/SEBS-*g*-MA blend, and PA6/SEBS-*g*-MA/nanotalc composites at $2\theta = 2°–35°$. [Color figure can be viewed in the online issue, which is available at wileyonlinelibrary.com.]

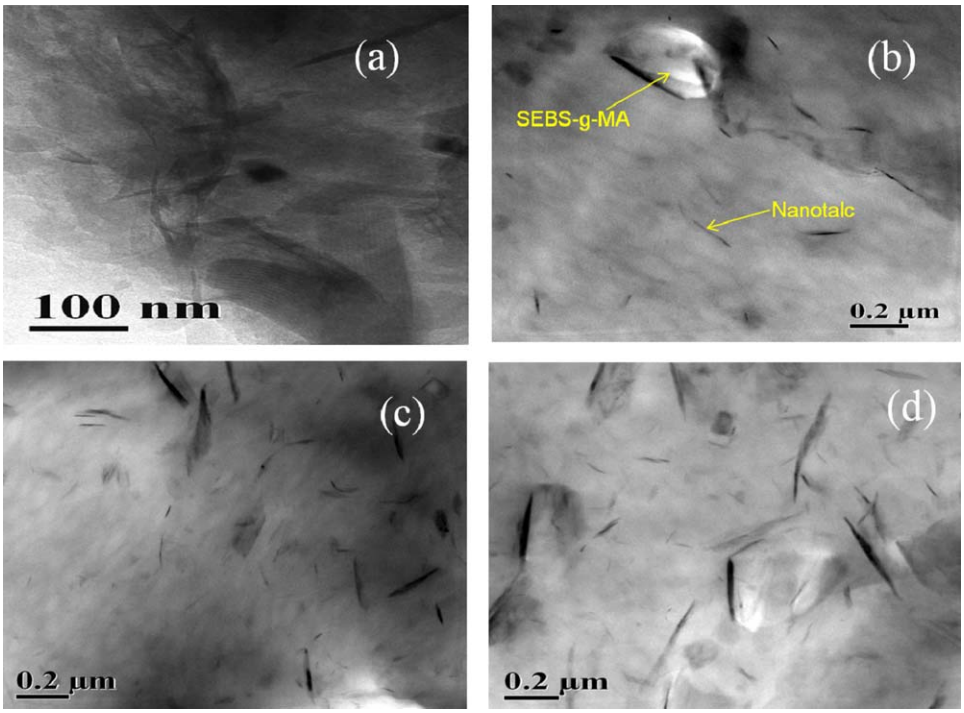

Figure 3. TEM images of (a) nanotalc, (b) NC1, (c) NC3, (d) NC5. [Color figure can be viewed in the online issue, which is available at wileyonlinelibrary.com.]

SEBS-*g*-MA.[72] PA6/SEBS-*g*-MA blend shows two dynamic relaxation peaks at −39 and 42°C referred to as β and α relaxation peak of SEBS-*g*-MA and PA6, respectively.[73] The β relaxation peak of PA6/SEBS-*g*-MA blend increased with the nanotalc content, indicating restricted chain mobility due to phase interaction. On the contrary, a diffuse pattern with two humps one at ~35°C temperature range and other at ~80°C have been observed for PA6/SEBS-*g*-MA nanocomposites. The appearance of these two peaks may be due to the reduced glass transition temperature of the β phase of PA6 and the PS phase of SEBS-*g*-MA, respectively. These results suggest that a polymer layer is formed around intercalated/exfoliated nanotalc.[74] Moreover, the peak width and intensity of tan δ are lower for nanocomposites than that of the blend matrix implying that intercalation/exfoliation of nanotalc in to PA6/SEBS-*g*-MA blend retards the mobility of polymer chains with temperature, which lowers hysteresis loss.[39]

Mechanical Properties

Tensile Properties. Tensile properties of PA6, PA6/SEBS-*g*-MA blend and the nanocomposites are enumerated in Table IV. The tensile modulus, tensile strength, flexural modulus, and flexural strength of PA6 decreased with the incorporation of SEBS-*g*-MA implying that PA6 matrix is substantially softened by low modulus SEBS-*g*-MA elastomer. The tensile modulus of blend matrix increases significantly while tensile strength shows marginal increase with the increase in talc content (Figure 5). The increase in modulus was by 50% while tensile strength enhanced by 24% as compared to the blend matrix. Thus reinforcing effect of nanotalc is implied, which is associated with two factors: good dispersion of talc in PA6/SEBS-*g*-MA matrix as demonstrated by HRTEM micrographs in Figure 3; second, the phase interaction between polar PA6, MA groups of SEBS-*g*-MA and hydrophilic nanotalc.[66] Nanotalc possesses OH groups, which octahedrally bind with the magnesium silicate. Since there is no cation in the interlayer, the possible interaction with PA6 may be through hydrogen bonding. The interaction of talc with PA6/SEBS-*g*-MA will facilitate stress transfer to talc layers which consequently improves tensile strength. However, the increase in tensile properties is less pronounced due to the presence of SEBS-*g*-MA elastomer.[39]

Impact Strength and Elongation-at-Break. The addition of SEBS-*g*-MA significantly improves the impact strength and elongation-at-break of PA6. The increase in impact strength with SEBS-*g*-MA content are presumably due to enhanced phase adhesion between PA6 and SEBS-*g*-MA, thus promoting better stress transfer.[75] Figure 6 depicts the effect of nanotalc on the impact strength and elongation-at-break of PA6/SEBS-*g*-MA blend. Addition of nanotalc into the blend matrix drastically decreases its impact strength and elongation-at-break. This may be attributed to the partially immobilized molecular chain by intercalation/exfoliation of nanotalc, which reduces the deformability of the blend leading to its fracture in brittle mode.[76]

The dispersed rubber particles in PA6 matrix cavitate easily to relieve the triaxial stress ahead of the advancing crack tips, which allows extensive shear yielding of PA6 matrix dissipating more energy thus enhancing the impact strength.[45] In the nanotalc filled composites the presence of nanotalc in the blend matrix creates stress concentration sites, which act as a micro crack initiator and reduces cavitation ability of the immobilized elastomer, leading to decreased impact strength.[77,78]

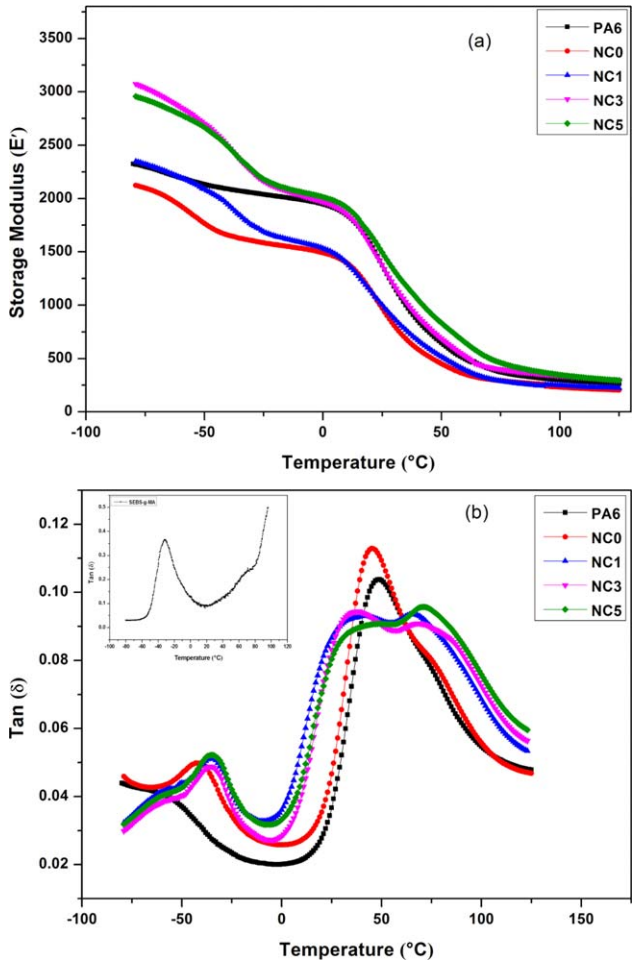

Figure 4. Dynamic mechanical properties of PA6, PA6/SEBS-*g*-MA blend and PA6/SEBS-*g*-MA nanocomposites as a function of temperature (a) storage modulus (b) Tan δ. [Color figure can be viewed in the online issue, which is available at wileyonlinelibrary.com.]

Flexural Properties. The variation of flexural modulus and flexural strength with nanotalc content are shown in Figure 7, Table IV. The flexural modulus of nanocomposites remarkably increased and flexural strength also increased as compared to blend matrix. This behavior resembles to that of the tensile properties. The increment in flexural properties could be attributed to the partially intercalated/exfoliated morphology and rigidifying effect of nanotalc on PA6/SEBS-*g*-MA matrix.

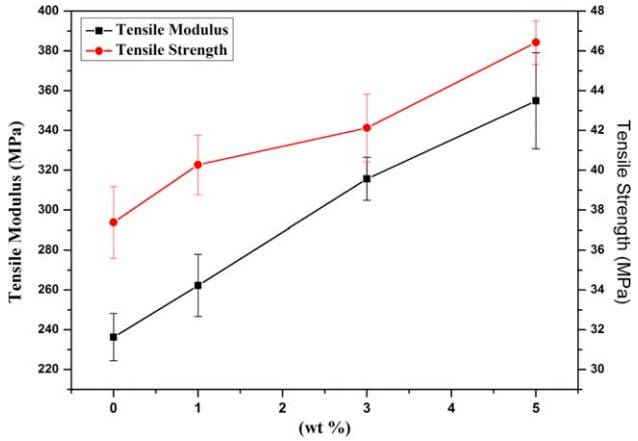

Figure 5. Variations of tensile modulus and tensile strength with nanotalc content. [Color figure can be viewed in the online issue, which is available at wileyonlinelibrary.com.]

Theoretical Modeling

Tensile Modulus. A micromechanical model has been developed for particulate filled polymer system to analyze the effects of filler geometry, orientation, and content along with the stress transfer efficiency in the nanocomposites. In the present investigation, Mooney model and Halpin–Tsai equation have been employed to analyze tensile modulus of the filled polymer system.

Mooney Model. Semiempirical Mooney model was used to predict the modulus of composites taking in to consideration of the shape and the aspect ratio of the reinforcing particles. The Mooney model was originally developed to study the effect of spherical fillers on the viscosity of a concentrated colloid fluid.[79] Extending the shape into nonspherical ones and taking its analogs of modulus of the filler, it was proposed that when the modulus of the filler is much higher than that of the modulus of the matrix, the increase can be described by the modified Mooney equation:[80]

$$ln\frac{E_c}{E_m} = K_E\left[\frac{\Phi_f}{1-\Phi_f/\Phi_m}\right] \quad (2)$$

where E_c and E_m represent young's modulli of nanocomposites and polymer matrix, respectively, Φ_f is the filler volume fraction and Φ_m is the maximum volume fraction that the filler can have ($\Phi_f = 0.637$).[81] K_E is the Einestein coefficient, which is a function of interaction between the matrix and the filler as well as the aspect ratio of the filler. The higher the K_E value the higher the aspect ratio and the better the interaction.

Table IV. Mechanical Properties of PA6, PA6/SEBS-*g*-MA, and PA6/SEBS-*g*-MA/Nanotalc Composites

Sample code	Tensile modulus (MPa)	Tensile strength (MPa)	Elongation-at-break (%)	Notched impact strength (J/m)	Flexural modulus (MPa)	Flexural strength (MPa)
PA6	266.3 ± 10.07	51.5 ± 0.9	105.5 ± 47.6	56.7 ± 0.4	3172.6 ± 113.2	100.5 ± 2.1
NC0	236.32 ± 11.9	37.38 ± 0.8	330.3 ± 30.4	425.15 ± 0.4	2353.8 ± 212.9	78.98 ± 3.4
NC1	262.29 ± 15.6	40.27 ± 1.5	280.8 ± 25.2	100.1 ± 3.7	3553.5 ± 255.3	100.7 ± 7.1
NC3	315.06 ± 10.8	42.13 ± 1.7	232.6 ± 28.5	89.8 ± 1.2	3913 ± 310.4	104.4 ± 6.1
NC5	354.94 ± 20.4	46.43 ± 1.1	189.1 ± 35.8	79.4 ± 2.8	4239.5 ± 290.3	107.3 ± 6.1

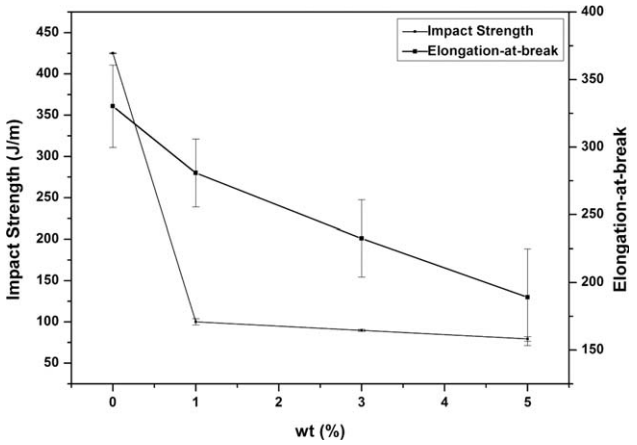

Figure 6. Variations of impact strength and elongation-at-break with nanotalc content.

By using eq (2), the aspect ratio (l/t) of nanotalc in PA6/SEBS-*g*-MA/nanotalc composites can be calculated as:

$$K_E = 2.5(L/t)^{0.645} \quad (3)$$

Halpin–Tsai Model. Halpin and Tsai developed a well sophisticated composite theory in the fibre composites to estimate the elastic stiffness moduli of unidirectional composites as a function of filler volume fraction and aspect ratio. In Halpin–Tsai model, filler geometry can be varied including discontinuous reinforcement such as fiber-like or flake-like fillers.[82,83] The theoretical prediction of young's modulus of composite materials in Halpin–Tsai model may be expressed as:

$$\frac{E_c}{E_m} = \frac{1+\zeta\eta\phi_f}{1-\eta\phi_f} \quad (4)$$

$$\eta = \left(\frac{E_f}{E_m} - 1\right) \Big/ \left(\frac{E_f}{E_m} + \zeta\right) \quad (5)$$

where E_c, E_f, and E_m represent young's modulli of composites, fillers and polymer matrix respectively, ϕ_f is the filler volume fraction and ζ is a shape factor parameter depending on filler geometry, orientation and loading direction. $\zeta = 2\ (l/d)$ for fibers or $2(l/t)$ for disc-like platelet in a particular direction,

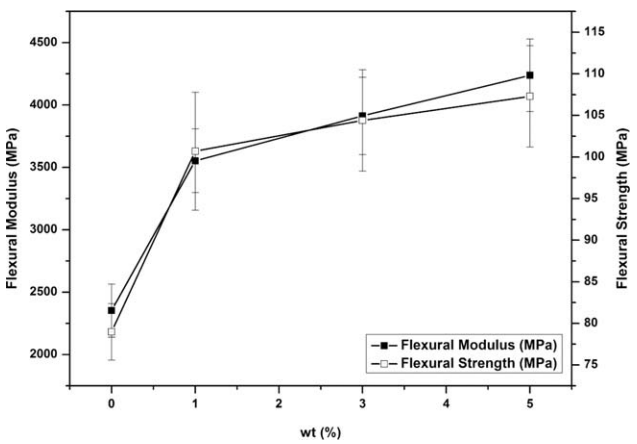

Figure 7. Variations of flexural modulus and flexural strength with the nanotalc content.

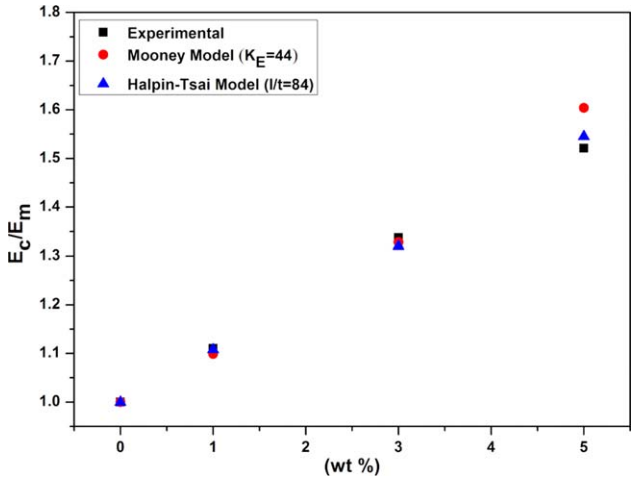

Figure 8. Plot of relative tensile modulus, E_c/E_m, of PA6/SEBS-*g*-MA and PA6/SEBS-*g*-MA/nanotalc composites with Mooney and Halpin–Tsai theoretical models as functions of nanotalc concentrations. [Color figure can be viewed in the online issue, which is available at wileyonlinelibrary.com.]

where l, d, t are the length, diameter, and thickness of the dispersed phase, respectively. Thus, the parameter η describes filler characteristics.

In these calculations, the tensile modulus of the blend matrix and the filler are taken as 236.3 MPa and 10 GPa,[84] respectively. According to Mooney model, eq. (2), the average value of K_E is 44, which were evaluated by comparing the experimental tensile modulus data with the predictive model. The aspect ratio of nanotalc for PA6/SEBS-*g*-MA/nanotalc composites is then calculated to be 84 from the Mooney eqs. (2) and (3), which were used in Halpin–Tsai equation to predict the tensile modulus of nanocomposites. The experimental data of relative tensile modulus as a function of nanotalc content are compared with the predictive eqs. (2–5) in Figure 8. The Mooney model shows good agreement for PA6/SEBS-*g*-MA/nanotalc composites at low weight fraction of talc (1 and 3%), whereas the model slightly overestimates at 5 wt % of nanotalc due to less interaction between the nanotalc and PA6/SEBS-*g*-MA. The Halpin–Tsai model also exhibits very good agreement with the modulus data implying the aspect ratio of nanotalc in composites evaluated by Mooney's equations was found to be a reasonable estimate for predicting the modulus. The Halpin–Tsai and Mooney models used in this study do not take in to account the aspect ratio of these structures formed by nanotalc reinforced composites. The aspect ratio has been calculated from the Mooney equation and the experimental values, which gives a value as 84. The aspect ratio in TEM micrographs seem to be lower due to the decrease in the parameter due to the shear involve in processing. The increase in modulus with the addition of talc may

Table V. Values of Interaction Parameters, B for PA6/SEBS-*g*-MA/Nanotalc Composites

Sample code	NC0	NC1	NC3	NC5	Mean value
B	-	25.83	15.08	16.56	19.15

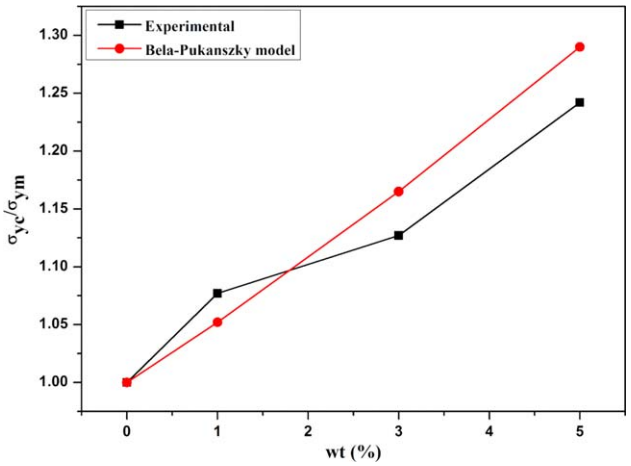

Figure 9. Plot of relative tensile strength, σ_{yc}/σ_{ym}, of PA6/SEBS-*g*-MA and PA6/SEBS-*g*-MA/nanotalc composites with Bela–Pukanszky model as a function of nanotalc (wt %). [Color figure can be viewed in the online issue, which is available at wileyonlinelibrary.com.]

be attributed to the surface interaction of the polymer with large surface area nanotalc.

Tensile Strength

Pukanszky Model. Pukanszky proposed the two phase composite model to analyze theoretical yield stress and the approach is based on the relationship between volume fraction (weight ratio) and area fraction of particulate inclusions[85,86]:

$$\sigma_{yc} = \sigma_{ym} \times \frac{1-\phi_f}{1+2.5\phi_f} exp\left(B\phi_f\right) \quad (6)$$

where σ_{yc} and σ_{ym} are the composites and matrix yield stress respectively, ϕ the volume fraction of talc in the composite. The fraction $\left(\frac{1-\phi_f}{1+2.5\phi_f}\right)$ expresses the effective load bearing cross-section of the matrix. At zero interaction, load bearing cross-section decreases with increasing filler content and the entire load is carried by the polymer.

B is an empirical parameter, which can be evaluated from the experimental data. The value of parameter *B* depends on all factors influencing the load bearing capacity of the filler i.e., strength of the interaction and size of the contact surface.

The values of parameter *B* for nanocomposites were evaluated by comparing the experimental tensile stress with the Pukanszky model. The values of parameter B, Table V, with a mean value 19.15 calculated for ternary PA6/SEBS-*g*-MA/nanotalc composites indicate good level of dispersion of nanotalc and better extent of reinforcing or load transfer efficiency. The values of *B* for a series of polyamide nanocomposites were reported to lie between 1.7 and 22.9, despite the fact in most similar cases, intercalated/exfoliated structure was claimed.[87] From Figure 9, it can be seen that the data show the positive deviation with the Pukanszky model at 1 wt % of nanotalc content while it show negative deviation at 3 and 5 wt % of nanotalc. This may be due to the exfoliation of nanotalc at 1 wt % in PA6/SEBS-*g*-MA matrix, which contribute more reinforcing effect and the partial intercalation/exfoliation of nanotalc at 3 and 5 wt % of nanotalc, which lead to an extent of decreased improvement in load bearing capacity.

CONCLUSION

Thermal stability of nanocomposites slightly improved in presence of nanotalc content. Morphology of PA6/SEBS-*g*-MA/nanotalc ternary nanocomposites investigated by TEM revealed the partially intercalation/exfoliation of nanotalc in blend matrix. WAXD did not show any diffraction peak of nanotalc indicating exfoliated talc structures. The presence of nanotalc changes the crystalline pattern of PA6 and promotes the γ-phase crystalline structure of PA6. DMA result shows that the storage modulus of blend matrix significantly improved over entire measured temperature range with the nanotalc content. The diffuse pattern of tan δ curve is observed due to partial exfoliation/intercalation of nanotalc in PA6 and SEBS-*g*-MA phase. The tensile modulus and strength of ternary nanocomposites increase, while ductility decreases with increase in nanotalc content. The experimental data of tensile modulus were compared with the Mooney and Halpin–Tsai models. The experimental data shows the good agreement with the applied models. This may be due to the some extent of phase interaction of silanol group of nanotalc with the polar amine group of PA6 and maleic anhydride group of SEBS-*g*-MA. Bela-Pukanskzy model was employed to interpret with the tensile yield stress data. The average value of parameter B evaluated by Bela-Pukanszky model is 19.15 indicating good load bearing capacity of nanocomposites.

ACKNOWLEDGMENTS

The authors acknowledge Council of Scientific and Industrial Research (CSIR) for providing financial assistance and V. Ramkrishnan (Technano materials) for providing nanotalc.

REFERENCES

1. Zanetti, M.; Lomakin, S.; Camino, G. J. *Macromol. Mater. Eng.* **2000**, *279*, 1.
2. Paul, D. R.; Robeson, L. M. *Polymer* **2008**, *49*, 3187.
3. Usuki, A.; Kojima, Y.; Kawasumi, M.; Okada, A.; Fukushima, Y.; Kurauchi, T. *J. Mater. Res.* **1993**, *8*, 1179.
4. Kojima, Y.; Usuki, A.; Kawasumi, M.; Okada, A.; Kurauchi, T.; Kamigaito, O. *J. Polym. Sci. Part A: Polym. Chem.* **1993**, *31*, 983.
5. Yano, K.; Usuki, A.; Okada, A. *J. Polym. Sci. Part A: Polym. Chem.* **1997**, *35*, 2289.
6. Orasa, K.; Rathanawan, M.; Johannes, W. S. *J. Appl. Polym. Sci.* **2003**, *89*, 2875.
7. Ke, Y.; Long, C.; Qi, Z. *J. Appl. Polym. Sci.* **1999**, *71*, 1139.
8. Ou, C. F.; Ho, M. T.; Lin, J. R. *J. Polym. Res.* **2003**, *10*, 127.
9. Hu, X.; Lesser, A. J. *J. Polym. Sci.: Polym. Phys. Ed.* **2003**, *41*, 2275.
10. Li, X.; Kang, T.; Cho, W. J.; Lee, J. K.; Ha, C. S.; *J. Macromol. Rapid. Commun.* **2001**, *22*, 1306.
11. Xiaohui, L.; Qiuju, W. *Polymer* **2001**, *42*, 10013.
12. GarceÇs, J. M.; Moll, D. J.; Bicerano, J.; Fibiger, R.; MacLeod, D. G. *J. Adv. Mater.* **2002**, *12*, 1835.

13. Sun, T.; GarceÇs, J. M. *J. Adv. Mater.* **2002**, *14*, 128.
14. Triantafillidis, C. S.; LeBaron, P. C.; Pinnavia, T. J. *J. Solid State Chem.* **2002**, *167*, 354.
15. Messersmith, P. B.; Giannelis, E. P. *J. Chem. Mater.* **1994**, *6*, 1719.
16. Wang, Z.; Pinnavaia, T. J. *J. Chem. Mater.* **1998**, *10*, 3769.
17. Kelnar, I.; Khunova, V.; Kotek, J.; KapraÇlkova, L. *Polymer* **2007**, *48*, 5332.
18. Unal, H.; Mimaroglu, A. *J. Reinf. Plast. Compos.* **2004**, *23*, 461.
19. Livi, S.; Duchet-Rumeau, J.; Thi Nhan, P.; Gerard, J. F. *J. Colloid Interface Sci.* **2011**, *354*, 555.
20. Rayner, J. H.; Brown, G. *J. Clays Clay Miner.* **1973**, *21*, 103.
21. Aglietti, E. F.; Lopez, P.; Jose, M. *J. Mater. Res. Bull.* **1992**, *27*, 1205.
22. Gaymans, R. J. In Rubber Toughened Engineering Plastics; Collyer, A. A., Eds.; Chapman & Hall: London, **1994**; Chapter 7, p 210.
23. Modic, M. J.; Pottick, L. A. *J. Polym. Eng. Sci.* **1993**, *33*, 819.
24. Wu, C. J.; Kuo, J. K.; Chen, C. Y. *J. Polym. Eng. Sci.* **1993**, *33*, 1329.
25. Oshinski, A. J.; Keskkula, H.; Paul, D. R. *Polymer* **1996**, *37*, 4919.
26. Lu, M.; Keshkula, H.; Paul, D. R. *J. Appl. Polym. Sci.* **1995**, *58*, 1175.
27. Kudva, R. A.; Keshkula, H.; Paul, D. R. *Polymer* **1998**, *39*, 2447.
28. Jafari, S. H.; Potschke, P.; Stephen, M.; Warth, H.; Alberts, H. *Polymer* **2002**, *43*, 6985.
29. Sun, S. L.; Tan, Z. Y.; Xu, X. F.; Zhou, C.; Ao, Y. H.; Zhang, H. X. *J. Appl. Polym. Sci.* **2005**, *43*, 2170.
30. Thomas, S.; Groeninkx, S. *J. Appl. Polym. Sci.* **1999**, *71*, 1405.
31. George, S. C.; Nihan, K. N.; Geuskens, G.; Sabu, T. *J. Appl. Polym. Sci.* **2004**, *91*, 3756.
32. Coltelli, M. B.; Passaglia, E.; Ciardeli, F. *Polymer* **2006**, *47*, 85.
33. Tanrattanakul, V.; Sungthong, N.; Raska, P. *J. Polym. Test.* **2008**, *27*, 794.
34. Wang, X.; Li, H.; Ruckenstein, E. *Polymer* **2001**, *42*, 9211.
35. Wang, W.; Zheng, Q.; *J. Mater. Sci.* **2005**, *40*, 5545.
36. Wu, S. *J. Polym. Sci.: Polym. Phys. Ed.* **1983**, *21*, 699.
37. Majumdar, B.; Keskkula, H.; Paul, D. R. *J. Appl. Polym. Sci.* **1994**, *54*, 339.
38. Oshinski, A. J.; Keskkula, H.; Paul, D. R. *Polymer* **1996**, *37*, 4909.
39. Tjong, S. C.; Bao, S. P. *J. Polym. Sci. Part B: Polym. Phys.* **2005**, *43*, 585.
40. Chiu, F. C.; Lai, S. M.; Chen, Y. L.; Lee, T. M. *Polymer* **2005**, *46*, 11600.
41. Mohanty, F. C.; Nayak, S. K. *J. Polym. Compos.* **2007**, *28*, 153.
42. Gonzalez, I.; Eguiazabal, J. I.; Nazabal, J. *J. Compos. Sci. Technol.* **2006**, *66*, 1833.
43. Gonzalez, I.; Eguiazabal, J. I.; Nazabal, J. *J. Polym. Sci. Part B* **2005**, *43*, 3611.
44. Gonzalez, I.; Eguiazabal, J. I.; Nazabal, J. *Eur. Polym. J.* **2008**, *44*, 287.
45. Ahn, Y. C.; Paul, D. R. *Polymer* **2006**, *47*, 2830.
46. Khatua, B. B.; Dong, J. L.; Hwang, Y. K.; Jin, K. K. *Macromolecules* **2004**, *37*, 2454.
47. Sharif, N. F. A.; Mohamad, Z.; Hassan, A.; Wahit, M. U. *J. Polym. Res.* **2011**, *19*, 9749.
48. He, S.; Wu, W.; Wang R. U.; Pu, W.; Chen, Y. *J. Polym. Plast. Technol. Eng.* **2011**, *50*, 719.
49. Balamurugan, G. P.; Maiti, S. N. *J. Polym. Eng. Sci.* **2010**, *50*, 1978.
50. Wang, K.; Wang, C.; Li, J.; Su, J.; Zhang, Q.; Du, R.; Fu, Q. *Polymer* **2009**, *48*, 2144.
51. Jannerfeldt, G.; Boogh, L.; Manson, J. A. E. *Polymer* **2000**, *41*, 7627.
52. ASTM standard D 638-41. Standard test method for tensile properties of plastics. West Conshohocken. American Society for Testing and Materials: Pennsylvania, **1941**.
53. ASTM standard D 790-70. Standard test methods for flexural properties of unreinforced and reinforced plastics and electrical insulating materials. American Society for Testing and Materials: West Conshohocken, Pennsylvania, **1970**.
54. ASTM standard D 256-26. Standard test methods for determining the Izod pendulum impact resistance of plastics. American Society for Testing and Materials: West Conshohocken, Pennsylvania, **1926**.
55. Gilman, J. W.; Jackson, C. L.; Morgan, A. B.; Harries, R.; Manias, E.; Giannelis, E. P. *J. Chem. Mater.* **2000**, *12*, 1866.
56. Araujo, E. M.; Leite, A. M. D.; daPaz, R. A.; Medeiros, V. D.; deMelo, T. J. A.; Lio, L. *Materials* **2011**, *4*, 1956.
57. Yousfi, M.; Livi, S.; Dumas, A.; Roux, C. L.; Crepin-Leblond, J.; Greenhill-Hooper, M.; Duchet-Rumeau. *J. Colloid Interface Sci.* **2013**, *403*, 29.
58. Samon, J. M.; Schultz, J. M.; Wu, J.; Hsiao, B.; Yeh, F.; Kolb, R. *J. Polym. Sci. Polym. Phys.* **1993**, *37*, 1277.
59. Schultz, J. M.; Hsiao, B.; Samon, J. M. *Polymer* **2000**, *41*, 8887.
60. Ramesh, C. E.; Gowd, B. *Macromolecules* **2001**, *34*, 3308.
61. Liu, L. M.; Qi, Z. N.; Zhu, X. G. *J. Appl. Polym. Sci.* **1999**, *71*, 1133.
62. Wu, T. M.; Liao, C. S. *J. Macromol. Chem. Phys.* **2000**, *201*, 2820.
63. Roux, C. L.; Martin, F.; Micoud, P.; Dumas, A. International Patent WO/2013/004979 (**2013**).
64. Katoh, Y.; Okamoto, M. *Polymer* **2009**, *50*, 4718.
65. Shan, G. Y.; Yang, W.; Xie, B. H.; Li, Z. M.; Chen, J.; Yang, M. B. *J. Polym. Test.* **2004**, *24*, 704.
66. Bilotti, E.; Zhang, R.; Deng, H.; Quero, F.; Fisher, H. R.; Peijs, T. *J. Compos. Sci. Technol.* **2009**, *69*, 2587.
67. Liu, T. X.; Liu, Z. M.; Ma, K. X.; Shen, L.; Zheng, K. Y.; He, C. B. *J. Compos. Sci. Technol.* **2003**, *63*, 331.
68. Zhao, Z.; Zheng, W.; Yu, W.; Tian, H.; Li, H. *J. Macromol. Rapid. Commun.* **2004**, *25*, 1340.

69. Chiu, F. C.; Lai, S. M.; Chen, Y. L.; Lee, T. M. *Polymer* **2005**, *46*, 11600.
70. Chow, W. S.; Mohd Ishak, Z. A.; Ishiaku, U. S.; Karger-Kocsis, J.; Apostolov, A. A. *J. Appl. Polym. Sci.* **2004**, *91*, 175.
71. Mohd Ishak, Z. A.; Berry, J. P. *J. Appl. Polym. Sci.* **1994**, *51*, 2145.
72. Ghosh, S.; Bhowmick, A. K.; Roychowdhury, N.; Holden, G. *J. Appl. Polym. Sci.* **2000**, *77*, 1621.
73. Liu, X.; Wu, Q.; Berglund, L. A.; Fan, J.; Qi, Z. *Polymer* **2001**, *42*, 8235.
74. Chow, W. S.; Mohd Ishak, Z. A.; Karger-Kocsis, J.; Apostolov, A. A.; Ishiaku, U. S. *Polymer* **2003**, *44*, 7427.
75. Arup, R. B.; Anup, K. G.; Ashok, M. *Polymer* **2001**, *42*, 9143.
76. Kusmono, Mohd Ishak, Z. A.; Chow, W. S.; Takeichi, T.; Rochmodi. *Compos. Part A* **2008**, *39*, 1802.
77. Dasari, A.; Yu, Z.-Z.; Mai, Y. W. *Polymer* **2005**, *46*, 5986.
78. Mareri, P.; Bastide, S.; Binda, N.; Crepsy, A. *Compos. Sci. Technol.* **1998**, *58*, 747.
79. Mooney, M. *J. Colloid. Sci.* **1951**, *6*, 162.
80. Rao, Y. Q.; Pochan, J. M. *J. Macromol.* **2007**, *40*, 290.
81. Bigg, D. M. *Polym. Compos.* **1987**, *8*, 115.
82. Halpin, J. C.; Kardos, J. L. *Polym. Eng. Sci.* **1976**, *16*, 344.
83. Fornes, T. D.; Paul, D. R. *Polymer* **2003**, *44*, 4993.
84. Martinatti, F.; Ricco, T. *J. Mater. Sci.* **1994**, *24*, 442.
85. Pukanszky, B.; Turcsanyi, B.; Tudus, F. In Effect of Interfacial Interaction on the Tensile Yield Stress of Polymer Composites, Ishida H., Ed. New York: Elsevier, **1988**; pp 467–477.
86. Turcsanyi, B.; Pukanszky, B.; Tudos, F. *J. Mater. Sci. Lett.* **1988**, *7*, 160.
87. Sazadi, L.; Pozsgay, A.; Pukanszky, B. *Eur. Polym. J.* **2007**, *43*, 345.